Materials Science & Engineering C 103 (2019) 109772

Contents lists available at ScienceDirect

Materials Science & Engineering C

journal homepage: www.elsevier.com/locate/msec

A miniaturized device for biomembrane permeation analysis

Dawei Ding[a], Jing Pan[b], Shih Hui Yeo[c], Vishal Wagholikar[d], Seng Han Lim[c], Chunyong Wu[e,*], Jerry Y.H. Fuh[d], Lifeng Kang[f,*]

[a] College of Pharmaceutical Sciences, Soochow University, 199 Ren'ai Road, Suzhou 215123, China
[b] Skinetrate Pte Ltd, 79 Ayer Rajah Crescent, Singapore 139955, Singapore
[c] Department of Pharmacy, National University of Singapore, 18 Science Drive 4, Singapore 117543, Singapore
[d] Department of Mechanical Engineering, National University of Singapore, 9 Engineering Drive 1, Singapore 117575, Singapore
[e] Department of Pharmaceutical Analysis, China Pharmaceutical University, 24 Tong Jia Xiang, Nanjing 210009, China
[f] School of Pharmacy, University of Sydney, Pharmacy and Bank Building A15, NSW 2006, Australia

ARTICLE INFO

Keywords:
Diffusion cell
3D printing
Transdermal drug delivery
Finite element method
Membrane

ABSTRACT

Transdermal drug delivery is widely investigated as an alternative drug administration route to oral delivery and hypodermic injections. Owing to the availability of human skin samples, *in vitro* tests are used to predict the *in vivo* delivery of transdermal drugs. The most widely used validation method is skin permeation using diffusion cells. Traditional diffusion cells, however, are capacious and often require large amounts of skin sample and drugs, which is undesirable, given the scarcity of new drug entities and the limitation of skin sample supply. In this study, we fabricated miniaturized multichannel devices (MCDs) by 3D printing, to minimize the use of skin and drug samples. The MCDs were compared with conventional static diffusion cells and achieved comparable drug permeation profiles. The finite element method-based simulation revealed the efficient carry-off of permeated ingredients by the multichannel devices, and a critical role of distance between the buffer stream and skin sample in determining the flow velocity inside the chamber. The results support these devices as qualified alternatives to Franz cells for *in vitro* permeation studies using biomembranes, with reduced use of skin and drug samples.

1. Introduction

Transdermal drug delivery systems, ranging from traditional formulations such as ointments, gels and patches, to novel micro/nanovehicles including micro/nanoemulsions [1], microneedles [2], liposomes and polymeric nanoparticles [3,4], are being increasingly studied as an alternative route of drug administration, due to its merits over oral delivery and hypodermic injections, namely, the avoidance of first-pass metabolism, relieved systemic side effects and toxicity, non-invasion and thus improved patient compliance [5–7]. To evaluate transdermal dosage forms, *in vitro* skin permeation testing can be used [8]. *In vitro* testing is envisioned to be increasingly necessary and vital, given the European Union's ban on the use of animals in cosmetic product testing, which potentially amplifies the demands of *in vitro* skin permeation testing. Besides therapeutic agents, such tests are also shedding light on the toxicity of a broad spectrum of chemicals that are potentially harmful to skin, such as pesticides, cosmetics and industrial organic solvents [9,10].

There are two types of diffusion cells, namely, static and flow-through cells, where biomembranes are placed between the donor and receptor compartments for testing [11,12]. Drugs in the donor compartment permeate through the biomembrane and are collected in the receptor medium. In a static cell (usually Franz cells), samples are withdrawn at predetermined intervals from the receptor compartment where the medium is mechanically stirred and replaced. Although widely used, Franz cells are vulnerable to the potential formation of unstirred water layer [13], which necessitates additional experiments and calculations to verify the results [14]. In flow-through cells, in contrast, receptor medium continuously flows through the receptor compartment and constantly removes the permeated analytes [8,12]. Compared to static cells, flow-through cells are capable of maintaining the sink condition, which is particularly useful for drugs with limited solubility in the receptor medium. Moreover, they are able to mimic the blood flow underneath the skin membrane, thus better representing the cutaneous physiological environment [12].

While both types of diffusion cells are useful for *in vitro* skin permeation testing, there are challenges. For one, they are generally capacious in diffusion areas (1–3 cm^2) and receptor volume (a few mL)

* Corresponding authors.
E-mail addresses: cywu@cpu.edu.cn (C. Wu), lifeng.kang@sydney.edu.au (L. Kang).

https://doi.org/10.1016/j.msec.2019.109772
Received 14 December 2018; Received in revised form 18 April 2019; Accepted 17 May 2019
Available online 18 May 2019
0928-4931/

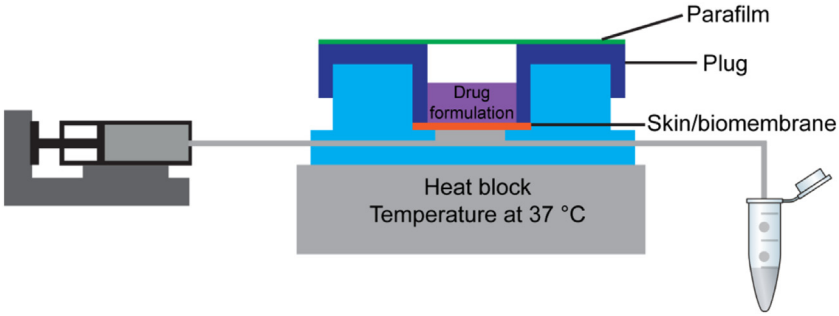

Fig. 1. Schematic representation of the MCD diffusion system (Side view of the diffusion cell).

[15], thus requiring a large amounts of skin and drug samples [11]. On the other hand, new investigative pharmaceutical ingredients, are often of limited supply and prohibitively expensive [11]. Consequently, it is of great importance to develop new devices which decrease the usage of drug and skin samples. To this end, companies such as PermeGear have developed diffusion cells with smaller diffusion area. Furthermore, microfluidic platforms have been incorporated into diffusion cells to reduce their size, such as the miniaturized flow-through cell (MFtC) [11] and multi-chamber devices [13]. In addition to their application in the *in vitro* cultivation of a wide range of tissues and their equivalents [16–19] which allow *in situ* drug screening and analysis, microfluidic platforms are also promising in increasing the through-put and reproducibility of skin permeation studies [13]. Nevertheless, their fabrication process is time-consuming and tedious, especially for channels of complex geometries since some of them depend on the multi-step soft lithography, which is usually limited by geometry complexity. Moreover, they are hindered by the low customizability. Any change or optimization in the diffusion cell design needs to reflect back to the original molds or photo-mask design, costing unpredictable time and efforts [11].

Recently, three dimensional (3D) printing or additive manufacturing, emerges as a versatile technology to revolutionize the product design and manufacturing of metals, ceramics, and polymers given their cost efficiency, ease of processing, high shape complexity, and potential high through-put, faster turnaround and customization to meet the demands of specific applications [7,20,21]. As 3D printing spreads recently from other technology sectors to medicine, it offers the capability to produce bio-printed tissues and customized medical prosthetics, implants, jigs and fixtures [21–23], which has a positive impact on the surgery procedure, success rate and patient recovery [21,24]. Recent years have also seen the applications of 3D printing technologies in drug delivery systems to pursue tailored release profiles and built-in flexibility that satisfies the needs of personalized medicines [25–27].

In this study, we use 3D printing to develop miniaturized flow-through multichannel devices (MCDs) to allow simultaneous testing of multiple replicates and more importantly to reduce the quantity of drug and skin samples required for *in vitro* testing. The devices were validated by skin permeation testing against conventional diffusion cells. In addition, the flow profiles and permeant concentration in MCDs were studied by using a Multiphysics model. The results show that the MCDs are qualified alternatives for *in vitro* skin permeation testing.

2. Materials and methods

2.1. Materials

Phosphate-Buffered Saline 10× (PBS) was purchased from Vivantis, Malaysia. Isopropyl alcohol (IPA), methanol and acetonitrile were obtained from Tedia, USA. Potassium dihydrogen phosphate was obtained from Alfa Aesar (Ward Hill, MA, USA). The photopolymer resin was purchased from Kuso3d Inc., USA.

2.2. Design, fabrication and assembly of MCDs

Three MCD models, MCD1, MCD2 and MCD3, were designed using AutoCAD® 2016 (San Rafael, USA). Each MCD is comprised of a main body with 6 identical receptor compartments, and 6 hollow plugs. The hollow plugs served as donor compartments and were designed to fit into the receptor compartments. Each model was printed with a 3D-printer (Titan 2, Kudo3D Inc., USA) by using Digital Light Processing Stereolithography (DLP-SLA) (see experimental details and Fig. S1 in Supplementary Information). The printed models were rinsed with IPA for 10 min to wash off excess resin before being exposed to ultra-violet (UV) light for 2 h for further curing. The models were then soaked in 70% (w/v) ethanol for 2 h to complete post processing. Polyethylene (PE) tubing (Braun, B, Germany) with an outer diameter of 1.9 mm were used to assemble the devices. The tubing was coated with a layer of epoxy glue at one end and inserted into each channel at the protruding parts of MCD. Afterwards, the other end of tubing was attached to the infusion syringes driven by a syringe pump or to sampling tubes (Fig. 1 and Fig. S2). The length of the PE tubing connecting MCD with sampling tube was minimized to ensure that the time of sample collection correlates better with the time of skin permeation [28].

2.3. Validation of MCDs

The MCDs were compared with Franz cells in a skin permeation study. Dermatomed human cadaver skin donated by a 67-year-old Caucasian male and a 61-year-old Caucasian female (Science Care, Pheonix, AZ, USA), were used in the testing of permeation of 2% lidocaine gel (Pfizer, West Ryde, Australia) and 1% diclofenac gel (diclofenac sodium) (Novartis, Nyon, Switzerland) respectively, under the approval by National University of Singapore Institutional Review Board. In the permeation tests using Franz cells, human cadaver skin of 1 in. by 1 in. was placed between the donor and receptor compartments, after which the drug was loaded into the donor compartments and 5 mL PBS and was loaded into the receptor compartment equipped with a Teflon-coated magnetic bar. The outlets of receptor were covered with parafilm to prevent water evaporation and the Franz cells were incubated in a temperature-controlled chamber set at 32 °C, which correlated with physiological temperature of human skin. Subsequently, at designated time intervals, 1 mL sample solution was withdrawn from the sampling tube and the remaining receptor medium was replaced with fresh PBS. In parallel, the MCDs were placed on a 37 °C heat block to maintain its actual temperature at 32 °C. Human cadaver skin sample of 8 mm diameter obtained by using an 8 mm skin biopsy punch (Acuderm Inc., USA), was placed into the receptor compartments. A plug was then placed onto the skin to fix the skin membrane. PBS was flushed into the system at 1 mL/min to fill the channels and remove air bubbles. Drugs were then added into the plug, which was covered by a piece of parafilm to prevent evaporation (Fig. 1a). The flow rate of PBS was set at 200 μL/h. The samples were collected at designated time points as stated above. There were 3 replicates for Franz cell testing, and 6 replicates for MCDs.

2.4. Simulation of flow and permeant concentration in MCDs

Simulation studies using a Multiphysics simulation model were undertaken to examine the flow conditions and to estimate the outlet concentrations in three MCDs based on the finite element method with same feed flow rates in each model. COMSOL Multiphysics software (v 5.2) was used for generating 3D mesh geometries and computation. The finite element mesh of the cells consisted of mixed type of elements. The meshing and solver details are provided in Supplementary Information. Laminar flow conditions were assumed in the flow chambers. Numerical simulation of flow in the cells is based on the Navier-Stokes and continuity equations as shown in Eqs. (1) and (2), respectively [29].

$$\rho_s\left(\frac{\partial \overline{u}}{\partial t} + \overline{u}\bullet\nabla\overline{u}\right) = -\nabla p + \mu\nabla^2\overline{u} + \overline{F_e} \quad (1)$$

$$\rho_s\nabla.\,(\overline{u}) = 0 \quad (2)$$

where p corresponds to the pressure, ρ_s is the density of the fluid, u is the flow velocity, μ is the dynamic viscosity and F_e resembles the external forces on the fluid due to gravity. No-slip conditions were applied at the cell/membrane surfaces and the fluid flow through the channels was assumed to be incompressible. Assuming the drug diffuses through the membranes with a given rate of flux (N_m) for all MCDs (that of lidocaine in Franz cells), the spatial distribution of the permeated drugs was modeled by the convection-diffusion equation [30] shown below in conjunction with the coupled velocity field from Eqs. (1) and (2).

$$\frac{\partial c}{\partial t} = \nabla.\,(\mathrm{D}\nabla c) - \nabla.\,(\overline{u}c) + N_m \quad (3)$$

where c is the concentration and D is the diffusion coefficient of the drug/chemical in water. The simulation parameters are shown in Table 1. The calculation method of mean outlet permeant concentration is provided in Supplementary Information.

2.5. Statistical analysis

One-way ANOVA was used to compare the skin permeation results of Franz cells and MCD. A p-value < 0.05 was considered significant.

3. Results and discussion

3.1. Design and fabrication of MCD

Recently 3D printing has been introduced to the production of drug delivery systems for tailored drug release [27,31,32]. In this study, it was used to fabricate three types of MCD with different geometries for skin permeation testing. The MCDs can deliver the permeation medium continuously through the receptor chamber (Fig. 1 and S2), mimicking the blood flow underneath the skins [12].

The design of MCD1 was an adaption from a previous study in which the surface in contact with the skin converges into a conical shape [11] (Fig. 2c). The limitation of MCD1 is that the small aperture of flow chamber constrained liquid flow. As a result, continuous replacement of PBS right below the skin may be compromised, leading to the loss of sink condition. Hence, two other designs were proposed, namely, MCD2 and MCD3, to improve liquid transportation. MCD2 makes use of a kink to drive PBS flowing upwards to the skin layer and remove the permeated drugs, while MCD3 features a cylindrical design (Fig. 2c).

With 3D printing, the dimensions and shapes of the resultant devices accurately replicated those of the AutoCAD® designs (Fig. 2a & b). In detail, the receptor compartment was 62 mm in length, 32 mm in width and 12 mm in height, while the cylindrical portion of the donor compartment was 11 mm in height, with an 8 mm outer diameter. The diffusion surface of MCDs was 4 mm in diameter, giving a diffusion area of 0.126 cm^2, which was 10 times smaller than that of Franz cell. This resulted in a miniaturized device (Fig. S3 and Table S1), which saves up to ~10 times of skin samples and/or drugs (Table S2). The biomembrane can be easily fixed by inserting the plugs into the devices (Figs. 1 and 2b). The device had 6 diffusion cells in parallel to meet the minimal replicates needed in pharmaceutical industry testing [12] (Fig. 2b). By adjusting the depth of insertion by the plugs, these devices can accommodate biomembranes of various thicknesses. Moreover, the process was quick (around 2 h), accurate and reproducible, with minimal variations in dimension. In addition, compared to our previous modeling method [11], the device parameters, such as chamber size and geometry, can be easily modified with 3D printing.

Table 1
Simulation parameters of MCD. The values of inlet flow rate and membrane flux are taken from this study. The difussion coefficient is taken from that of small molecules in water for simplicity and that's a constant in the simulation.

Parameter	Unit	Value
Inlet flow rate, u	μL/h	200
Diffusion coefficient, D	m^2/s	1×10^{-9}
Membrane flux, N_m	mol/(m^2 s)	3×10^{-7}

3.2. Validation of MCD

To validate the MCDs, *in vitro* permeation studies were performed over 24 h to compare the drug permeation profile obtained from the MCDs with that from conventional Franz cells (Fig. 3). A low flow rate at 0.2 mL/h was used to achieve minimal permeant concentration in the receptor solution for analysis [11] and to mimic the *in vivo* sink condition in skin due to cutaneous blood flow [12].

Two commercial topical formulae, namely, 1% diclofenac gel and 2% lidocaine gel, were used for the testing. No significant differences ($p > 0.05$) were found between the various MCDs and Franz cells (Fig. 3a and b), although the permeation profile of diclofenac for MCD2 was slightly higher than the others (Fig. 3a). These results suggest that the MCDs, especially MCD1 and MCD3 are promising platforms for the skin permeation investigations. We also observed that the skin permeation rates of both drugs were much higher than that reported in pure solution [33,34]. This may be due to the presence of permeation enhancers in the gel formula [35]. We also found that the total amount of penetrated lidocaine was much higher than diclofenac in 24 h. This is likely due to the differences in their concentrations (diclofenac 1% and lidocaine 2%) and other factors, such as molecular weight and lipophilicity of drugs [36–38].

No significant difference was found between Franz cells and all MCDs in the comparison of the percentage of drug that permeated in 24 h. The permeation percentage of MCD2 for diclofenac within 24 h was slightly higher than others (Fig. 3c), which could be attributed to the drug solubility in the receptor medium. In flow-through cells, the increased partitioning of compounds from skin to the receptor medium, due to continuous replacement of receptor medium, may result in greater permeation than in static cells [39–41], as discussed in the below.

We then examined the flux of both drugs, which could be influenced by a range of parameters, including receptor volume, flow rate, sampling frequency and volume [42]. There was no statistically significant difference between Franz cells and the MCDs, which is ~2 and 40 μg/(cm^2 h) for diclofenac and lidocaine, respectively (Fig. 3d and inset). Taken together, these data suggest that MCDs could serve as eligible alternatives to Franz cells for skin permeation testing. As validated devices for the skin permeation testing, we also believe the MCDs are promising and qualified candidates for the permeation/absorption evaluation of other biomembranes and equivalents such as bladder wall [43] and artificial intestines [44], amniotic membrane [45], pulmonary cell layers [46], blood brain barrier [47] *etc.*, as a tool to benefit drug

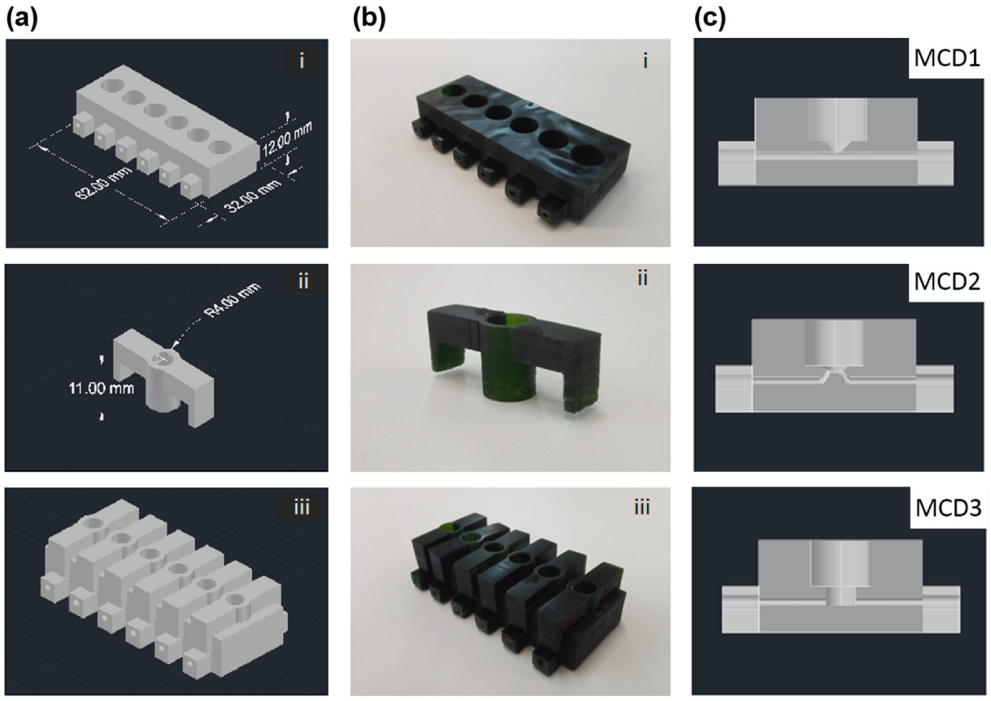

Fig. 2. (a) The AutoCAD© schematic representations of the MCD design. i): the bottom with receptor chamber; ii): the top inset with donor compartment; iii): the overview of whole device. (b) The image of an MCD corresponding to the design shown in (a). (c) The various designs of receptor chambers.

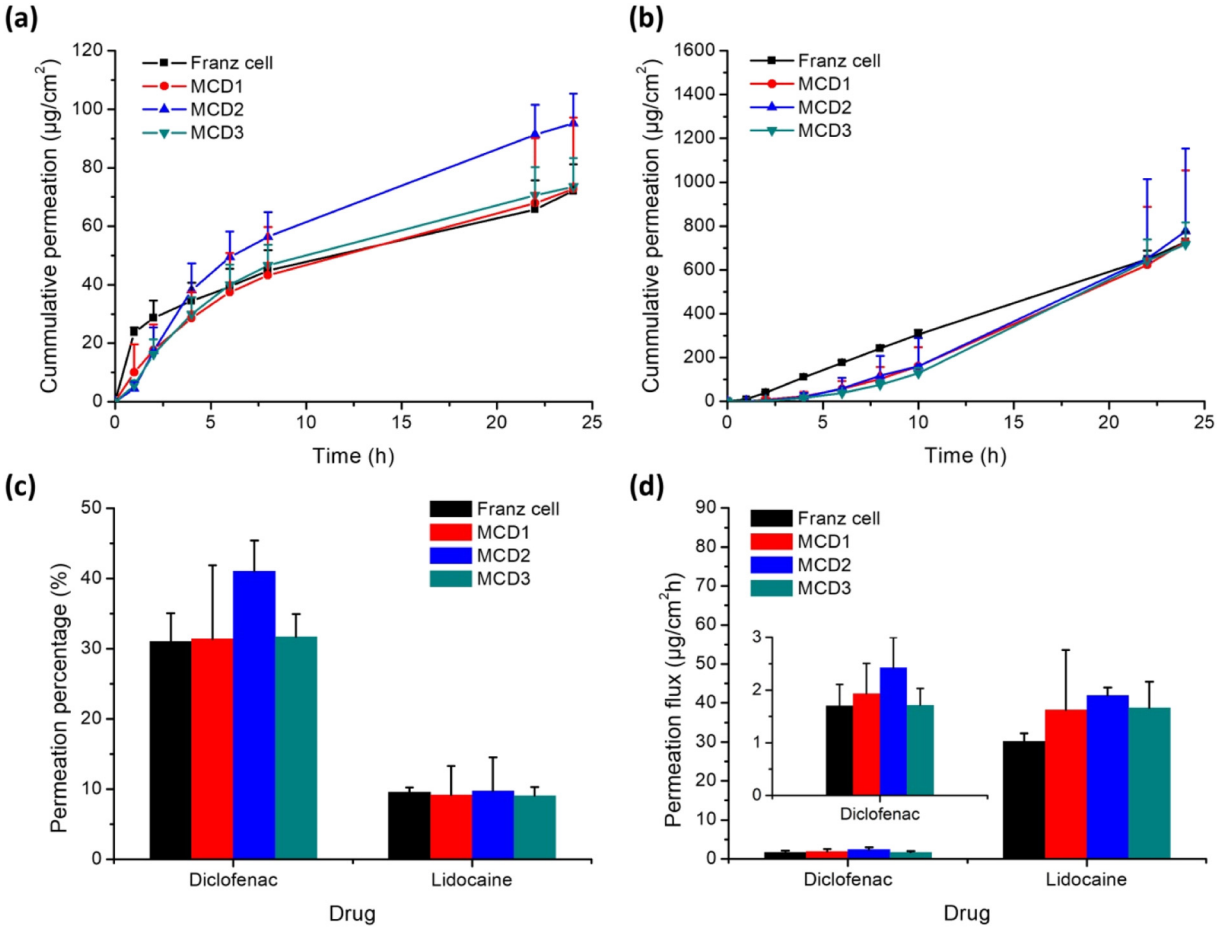

Fig. 3. The permeation profiles diclofenac (a) and lidocaine (b). (c) Percentage of drugs permeated through the skins with various devices. There is no significant difference in percentage permeation against Franz cells for MCDs ($p > 0.05$). (d) Permeation flux between Franz cells and MCDs. The inset shows the flux of diclofenac. There is no significant difference against Franz cells for MCDs ($p > 0.05$).

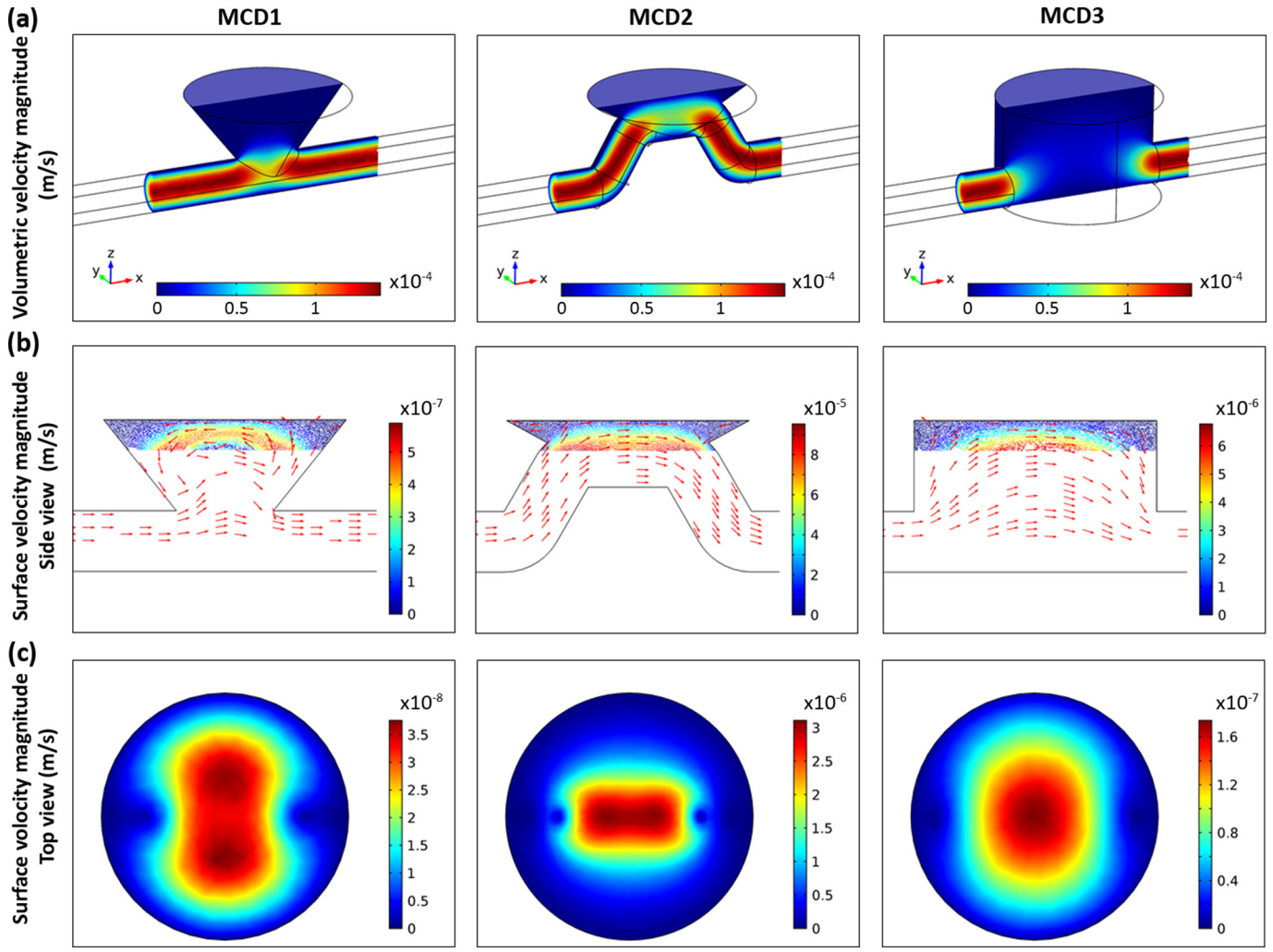

Fig. 4. The simulation study of 3 MCD models at a flow rate of 200 μL/h. (a) Volumetric flow velocities in the chamber and tubing. (b) The zoomed-in vertical velocity profiles at the proximity to the top (skin sample). The area close to the main stream at the bottom is not displayed due to the much higher magnitude of velocity. The red arrows showed the velocity directions. (c) The top surface velocity profiles of MCDs at a distance of 10 μm from the skin sample. (For interpretation of the references to colour in this figure legend, the reader is referred to the web version of this article.)

screening and discovery since they could also potentially save the usage of compounds and biomembranes in those testing.

3.3. Simulation of flow rate and permeant accumulation inside MCD

To examine how the permeated drug was removed by the continuous flow, COMSOL was used to simulate the flow velocity and drug concentration in the MCDs. Numerical simulation was widely used in medicine-related applications [48,49], but it has yet to be used in the study of drug permeation, to the best of our knowledge.

In general, all results displayed the volumetric gradients of flow velocities at the cross-sections inside the receptor chambers (Fig. 4a). In MCD1, there were certain apparent flows inside the receptor chamber, but those were primarily at the bottom of chamber and the flow rates significantly decreased towards the chamber top surface to form a thick layer of less-mixed medium, which would potentially limit the efficiency of mass exchange. MCD3 also showed gradually decreased flow rates towards the skin position (Fig. 4a). In MCD2, on the other hand, the flow rates were apparently higher due to the presence of kinks and the proximity of the bulk flow to the skin samples. MCD2 itself has a narrower gradient of flow velocity than the other two, leading to a very thin layer of less-mixed medium and much higher flow velocities right underneath the skin samples.

A closer examination at the top regions close to the skin samples revealed more than one order of magnitude higher flow velocities of MCD2 compared to MCD1 and MCD3, while that of MCD3 was much higher than MCD1 (Fig. 4b). In addition, we also noticed different profiles of flow directions among various MCDs attributed to their variances in chamber dimension and geometry. A narrower space of MCD2 resulted in flows parallel to the skin sample, while MCD3 experienced some parallel flow expansion due to the rectangular chamber. On the other hand, MCD1 created a lot of backflows close to the skin samples. It's interesting to notice that a bigger conical shape of chamber was capable of creating apparent backflows, while neither a cylindrical chamber with the same height nor a conical chamber with smaller height was able to achieve that, indicating the cooperative role of narrowing-down and chamber height in producing secondary flows for deeper chambers.

In terms of absolute flow velocity close to the skin positions (a distance of 10 μm from the skins) in the top view among diverse designs (Fig. 4c), MCD2 displayed generally much faster flows than MCD1 and MCD3, while the latter two also showed differences between themselves. The shapes of relatively high velocity regions (from red to yellow coding) differed from spindle to ellipse depending on the MCD designs, while maxima of flow rate for each MCD were around 0.04, 3 and 0.18 μm/s, respectively. This is not only in accordance with the

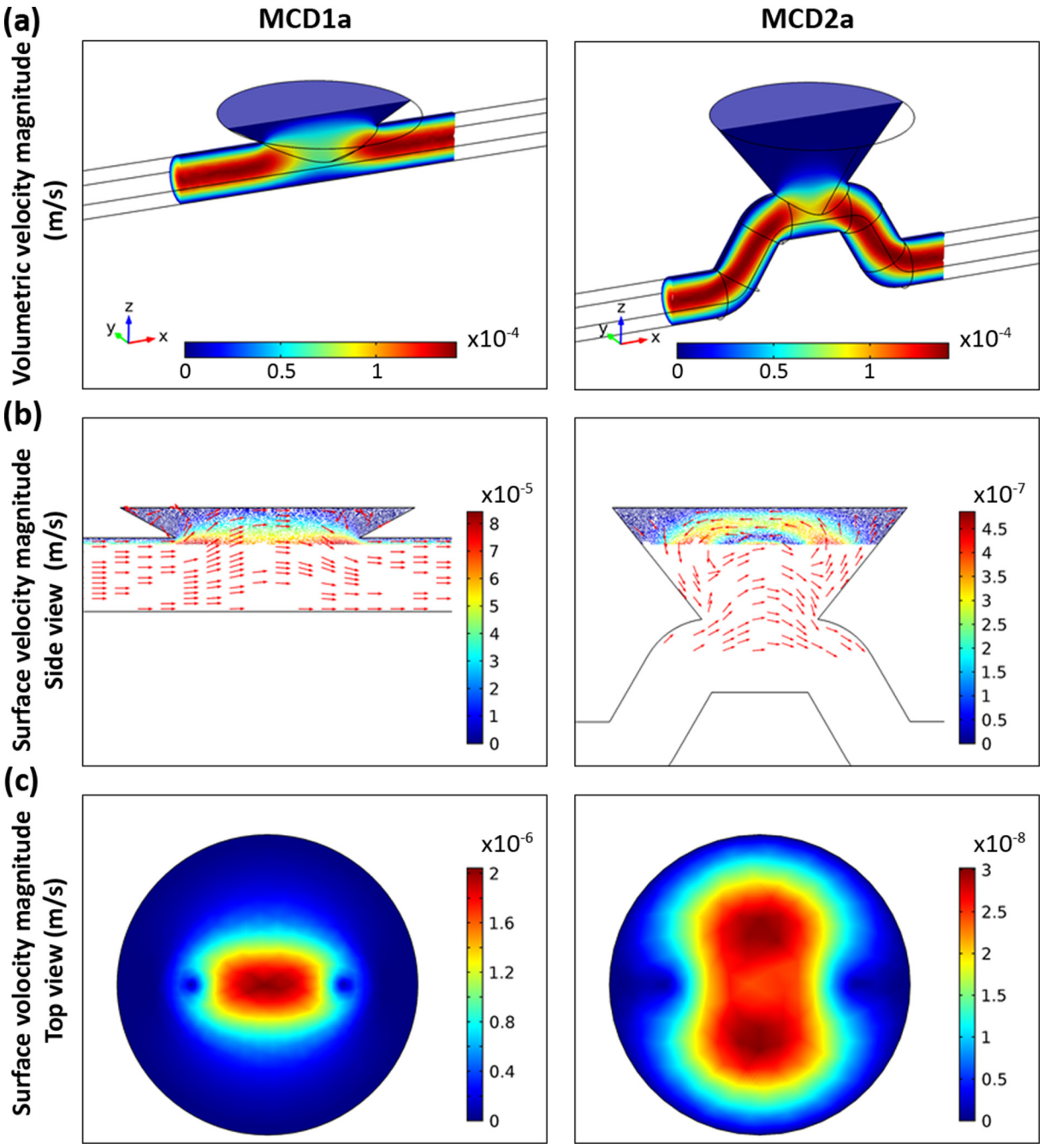

Fig. 5. The simulation study of three MCD1a and MCD2a at a flow rate of 200 μL/h. (a) Volumetric flow velocities in the chamber and tubing. (b) The zoomed-in vertical velocity profiles at the proximity to the top (skin sample). The red arrows showed the velocity directions. (c) The top surface velocity profiles of MCDs at a distance of 10 μm from the skin sample. (For interpretation of the references to colour in this figure legend, the reader is referred to the web version of this article.)

comparison of flow velocity in the vertical direction (Fig. 4b), but also endorsing the relatively higher permeation and drug flux for MCD2 than for the other two (Fig. 3).

To find out the key factor leading to the higher flow rate in MCD2, two additional models were simulated, namely, MCD1a and MCD2a. MCD1a has no kink, and has the same distance between the inlet and the skin sample as MCD2. On the other hand, MCD2a has a kink and has the same distance between the inlet and the skin sample as MCD1 (Fig. 5).

Interestingly, the flow rate right underneath the skin of MCD2a was significantly lower than that of MCD2 but displaying a flow pattern of comparable to MCD1. By examining the design of MCD1 and MCD2a closely, it can be observed immediately that the MCD2a resembled MCD1, in terms of the positions of inlet and outlet, which explains their almost identical flow velocities.

On the other hand, MCD1a displayed a comparable profile of flow velocity to that of MCD2, but largely different from that of MCD1. The results combined to suggest that the distance between the flowing-in position of buffer and skin sample is the key factor giving rise to the high flow rates, while the existence of kink in the assembly plays a marginal role.

MCD1a and MCD2 are the preferred designs because faster flow can remove the permeants at a faster rate to maintain the sink condition inside the receptor chamber. In the actual product design, however, MCD1a may not be useful because the resultant donor compartment will have a very thin bottom, which is easily broken.

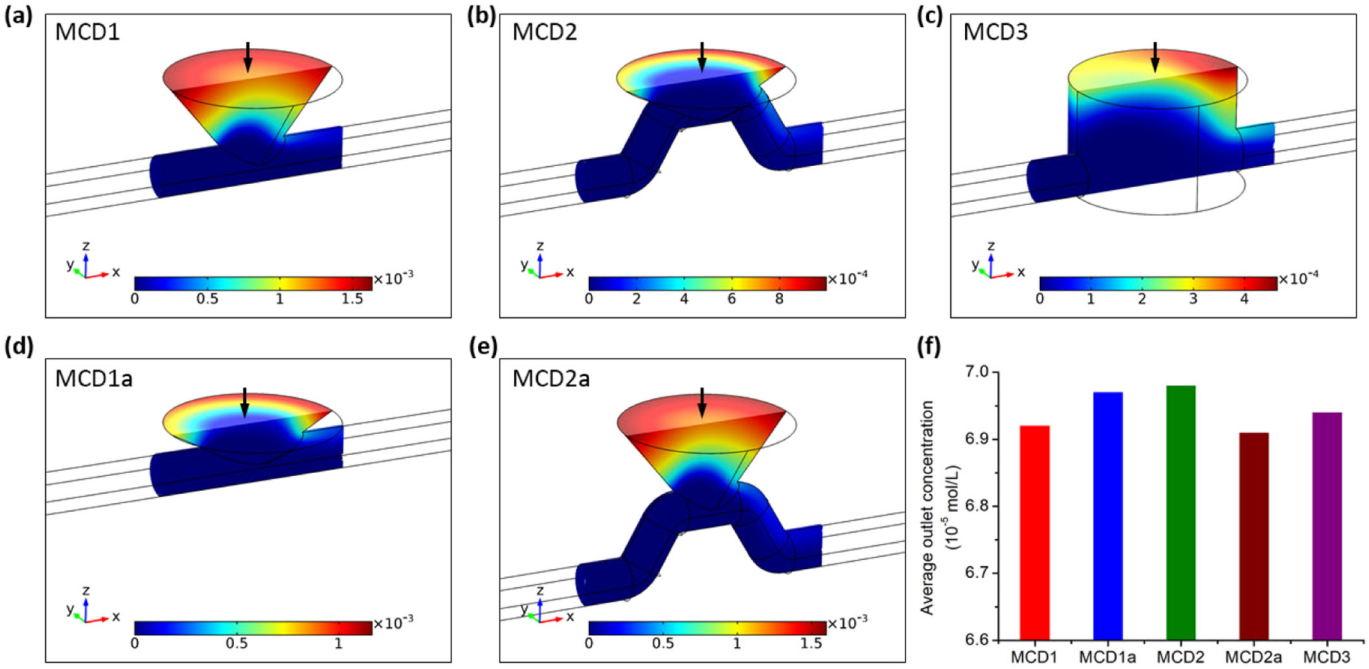

Fig. 6. Simulation results for the determination of drug accumulation in the MCD receptor chamber. (a–e) Simulated drug concentration in the MCD1 to MCD3: the mass accumulates in the receptor towards the outlet channel. The arrows show the direction of ingredient permeation. (f) Average outlet drug concentrations for different MCDs.

Finally, we estimated the outlet concentrations in the MCDs by comparing the concentration distributions of drugs permeated through skin using the numerical simulations. With an identical permeation flux as that in Franz cells, the permeated drugs were more efficiently removed by PBS in MCD2 and MCD1a than in the other three MCDs (Fig. 6a–e), which was in agreement with the distribution of flow velocities, especially high velocities underneath the skins discussed above. This led to a slightly higher average outlet drug concentration for MCD2 than for MCD1 and MCD3 (Fig. 6f), and was consistent with the slightly higher permeation and drug flux of MCD2 than the other two in the permeation tests (Fig. 3a and b), since a faster clearance of permeants through the skin in MCD2 would create a better sink condition.

In addition, we also noticed that the permeant concentration profile of MCD1 was comparable to MCD2a while MCD2 and MCD1a shared a similar profile. These results were in agreement with their respective flow velocity profiles in the receptor chambers of MCDs. Taken together, the profiles of both flow velocity and permeant concentrations suggested the critical role of distance between main buffer streams and skin samples. It's also worth to mention an asymmetric permeant concentration from left to right for MCD1a, MCD2 and MCD3, while that of MCD1 and MCD2a was relatively symmetric. The symmetry was believed to result from the mixing of backflow created by the specific chamber geometry for the later tow (Figs. 4b and 5b).

Collectively, the findings in this study not only relieve the immediate scarcity of skins and reagents with scaled-down devices produced by convenient and high-throughput 3D printing method in skin permeation studies of various therapeutics and other chemicals such as cosmetics and organic solvents, but also pave the way for the design of flow-through diffusion cells in long term, which has been largely overlooked. Besides skin permeation, MCDs could also find their applications in the permeation or absorption investigation of other biomembranes and their equivalents from bladder wall to artificial intestine models, amniotic membranes, and blood brain barriers, which could potentially benefit drug screening and discovery.

4. Conclusions

In summary, 3D printing has been used to fabricate three miniaturized MCDs with 6 microchannels in a device. Their performances were verified by *in vitro* skin permeation testing against Franz cells. Importantly, the MCDs were able to save ~10 folds of skins and/or drugs. All MCDs displayed no statistical difference in permeation profiles and flux compared to Franz cells, suggesting they could be used as the eligible alternatives for *in vitro* skin permeation testing. We also performed numerical simulation using the finite element method to investigate the profiles of flow velocities and estimate the outlet concentrations in each MCD. Different designs revealed various flow rate gradients in the chambers. Strikingly, we found the geometry of receptor chambers, particularly the proximity between the buffer inlet and the skin sample played a critical role in determining the ultimate flow rate right underneath the skins and how the permeated drugs are carried away, in agreement with the difference between MCDs in permeation studies.

Acknowledgements

We acknowledge the start-up funding from Soochow University, the National Research Foundation of Singapore through SMART center's BioSyM IRG research program, and an AcRF Tier 1 grant (R148-000-224-112) from Ministry of Education, Singapore.

Declaration of competing interest

The authors declare no conflict of interest.

Appendix A. Supplementary data

Supplementary data to this article can be found online at https://doi.org/10.1016/j.msec.2019.109772.

References

[1] M. Gibson, Pharmaceutical Preformulation and Formulation: A Practical Guide from Candidate Drug Selection to Commercial Dosage Form, CRC Press, Boca Raton, 2016, pp. 475–525.
[2] D. Ding, J. Pan, S.H. Lim, S. Amini, L. Kang, A. Miserez, Squid suckerin microneedle arrays for tunable drug release, J. Mater. Chem. B 5 (2017) 8467–8478.
[3] D. Ding, Q. Zhu, Recent advances of PLGA micro/nanoparticles for the delivery of biomacromolecular therapeutics, Mater. Sci. Eng. C 92 (2018) 1041–1060.
[4] O. Uchechi, J.D.N. Ogbonna, A.A. Attama, Nanoparticles for dermal and transdermal drug delivery, in: A.D. Sezer (Ed.), Application of Nanotechnology in Drug Delivery, InTech, Rijeka, 2014, pp. 193–235.
[5] M.R. Prausnitz, R. Langer, Transdermal drug delivery, Nat. Biotechnol. 26 (2008) 1261–1268.
[6] S.F. Ng, J.J. Rouse, F.D. Sanderson, V. Meidan, G.M. Eccleston, Validation of a static Franz diffusion cell system for in vitro permeation studies, AAPS PharmSciTech 11 (2010) 1432–1441.
[7] S.N. Economidou, D.A. Lamprou, D. Douroumis, 3D printing applications for transdermal drug delivery, Int. J. Pharm. 544 (2018) 415–424.
[8] H. Tanojo, P.E.H. Roemelé, G.H. van Veen, H. Stieltjes, H.E. Junginger, H.E. Boddé, New design of a flow-through permeation cell for studying in vitro permeation studies across biological membranes, J. Control. Release 45 (1997) 41–47.
[9] H.E. Buist, G. Schaafsma, J.J. van de Sandt, Relative absorption and dermal loading of chemical substances: consequences for risk assessment, Regul. Toxicol. Pharmacol. 54 (2009) 221–228.
[10] M.A. Ngo, M. O'Malley, H.I. Maibach, Percutaneous absorption and exposure assessment of pesticides, J. Appl. Toxicol. 30 (2010) 91–114.
[11] C.S. Mah, J.S. Kochhar, P.S. Ong, L. Kang, A miniaturized flow-through cell to evaluate skin permeation of endoxifen, Int. J. Pharm. 441 (2013) 433–440.
[12] L. Bartosova, J. Bajgar, Transdermal drug delivery in vitro using diffusion cells, Curr. Med. Chem. 19 (2012) 4671–4677.
[13] M. Alberti, Y. Dancik, G. Sriram, B. Wu, Y.L. Teo, Z. Feng, M. Bigliardi-Qi, R.G. Wu, Z.P. Wang, P.L. Bigliardi, Multi-chamber microfluidic platform for high-precision skin permeation testing, Lab Chip 17 (2017) 1625–1634.
[14] M.A. Miller, G. Kasting, A measurement of the unstirred aqueous boundary layer in a Franz diffusion cell, Pharm. Dev. Technol. 17 (2012) 705–711.
[15] M.R. Prausnitz, S. Mitragotri, R. Langer, Current status and future potential of transdermal drug delivery, Nat. Rev. Drug Discov. 3 (2004) 115–124.
[16] B. Atac, I. Wagner, R. Horland, R. Lauster, U. Marx, A.G. Tonevitsky, R.P. Azar, G. Lindner, Skin and hair on-a-chip: in vitro skin models versus ex vivo tissue maintenance with dynamic perfusion, Lab Chip 13 (2013) 3555–3561.
[17] I. Maschmeyer, A.K. Lorenz, K. Schimek, T. Hasenberg, A.P. Ramme, J. Hubner, M. Lindner, C. Drewell, S. Bauer, A. Thomas, N.S. Sambo, F. Sonntag, R. Lauster, U. Marx, A four-organ-chip for interconnected long-term co-culture of human intestine, liver, skin and kidney equivalents, Lab Chip 15 (2015) 2688–2699.
[18] S.N. Bhatia, D.E. Ingber, Microfluidic organs-on-chips, Nat. Biotechnol. 32 (2014) 760–772.
[19] B.L. Khoo, G. Grenci, T. Jing, Y.B. Lim, S.C. Lee, J.P. Thiery, J. Han, C.T. Lim, Liquid biopsy and therapeutic response: circulating tumor cell cultures for evaluation of anticancer treatment, Sci. Adv. 2 (2016) e1600274.
[20] S.C. Ligon, R. Liska, J. Stampfl, M. Gurr, R. Mulhaupt, Polymers for 3D printing and customized additive manufacturing, Chem. Rev. 117 (2017) 10212–10290.
[21] C.L. Ventola, Medical applications for 3D printing: current and projected uses, Pharmacol. Ther. 39 (2014) 704–711.
[22] A.A. Giannopoulos, D. Mitsouras, S.J. Yoo, P.P. Liu, Y.S. Chatzizisis, F.J. Rybicki, Applications of 3D printing in cardiovascular diseases, Nat. Rev. Cardiol. 13 (2016) 701–718.
[23] J. Banks, Adding value in additive manufacturing: researchers in the United Kingdom and Europe look to 3D printing for customization, IEEE Pulse 4 (2013) 22–26.
[24] L. Mertz, Dream it, design it, print it in 3-D: what can 3-D printing do for you? IEEE Pulse 4 (2013) 15–21.
[25] A. Goyanes, J. Wang, A. Buanz, R. Martinez-Pacheco, R. Telford, S. Gaisford, A.W. Basit, 3D printing of medicines: engineering novel oral devices with unique design and drug release characteristics, Mol. Pharm. 12 (2015) 4077–4084.
[26] A.H. Jassim-Jaboori, M.O. Oyewumi, 3D printing Technology in Pharmaceutical Drug Delivery: prospects and challenges, J. Biomol. Res. Ther. 4 (2015) 1000e141.
[27] J. Goole, K. Amighi, 3D printing in pharmaceutics: a new tool for designing customized drug delivery systems, Int. J. Pharm. 499 (2016) 376–394.
[28] W.J. Addicks, G.L. Flynn, N. Weiner, Validation of a flow-through diffusion cell for use in transdermal research, Pharm. Res. 4 (1987) 337–341.
[29] L. Gurreri, A. Tamburini, A. Cipollina, G. Micale, M. Ciofalo, CFD prediction of concentration polarization phenomena in spacer-filled channels for reverse electrodialysis, J. Membr. Sci. 468 (2014) 133–148.
[30] Z. Chai, T.S. Zhao, Lattice Boltzmann model for the convection-diffusion equation, Phys. Rev. E 87 (2013) 063309.
[31] S.A. Khaled, J.C. Burley, M.R. Alexander, J. Yang, C.J. Roberts, 3D printing of five-in-one dose combination polypill with defined immediate and sustained release profiles, J. Control. Release 217 (2015) 308–314.
[32] S.H. Lim, S.M.Y. Chia, L. Kang, K.Y.L Yap, Three-dimensional-printing of carbamazepine sustained-release scaffold, J. Pharm. Sci. 105 (2016) 2155–2163.
[33] M.J. Kim, H.J. Doh, M.K. Choi, S.J. Chung, C.K. Shim, D.D. Kim, J.S. Kim, C.S. Yong, H.G. Choi, Skin permeation enhancement of diclofenac by fatty acids, Drug Deliv. 15 (2008) 373–379.
[34] J. Stahl, M. Kietzmann, The effects of chemical and physical penetration enhancers on the percutaneous permeation of lidocaine through equine skin, BMC Vet. Res. 10 (2014) 138.
[35] M.E. Lane, Skin penetration enhancers, Int. J. Pharm. 447 (2013) 12–21.
[36] M. Hagen, M. Baker, Skin penetration and tissue permeation after topical administration of diclofenac, Curr. Med. Res. Opin. 33 (2017) 1623–1634.
[37] M.B. Brown, G.P. Martin, S.A. Jones, F.K. Akomeah, Dermal and transdermal drug delivery systems: current and future prospects, Drug Deliv. 13 (2006) 175–187.
[38] B.M. Magnusson, Y.G. Anissimov, S.E. Cross, M.S. Roberts, Molecular size as the main determinant of solute maximum flux across the skin, J. Investig. Dermatol. 122 (2004) 993–999.
[39] R.L. Bronaugh, R.F. Stewart, Methods for in vitro percutaneous absorption studies IV: the flow-through diffusion cell, J. Pharm. Sci. 74 (1985) 64–67.
[40] P. Kumar, P. Sanghvi, C.C. Collins, Comparison of diffusion studies of hydrocortisone between the Franz cell and the enhancer cell, Drug Dev. Ind. Pharm. 19 (1993) 1573–1585.
[41] R.L. Bronaugh, R.F. Stewart, Methods for in vitro percutaneous absorption studies III: hydrophobic compounds, J. Pharm. Sci. 73 (1984) 1255–1258.
[42] J. Sclafani, J. Nightingale, P. Liu, T. Kurihara-Bergstrom, Flow-through system effects on in vitro analysis of transdermal systems, Pharm. Res. 10 (1993) 1521–1526.
[43] I. Grabnar, M. Bogataj, A. Mrhar, Influence of chitosan and polycarbophil on permeation of a model hydrophilic drug into the urinary bladder wall, Int. J. Pharm. 256 (2003) 167–173.
[44] Y. Imura, Y. Asano, K. Sato, E. Yoshimura, A microfluidic system to evaluate intestinal absorption, Anal. Sci. 25 (2009) 1403–1407.
[45] D.H. Ma, J.Y. Lai, H.Y. Cheng, C.C. Tsai, L.K. Yeh, Carbodiimide cross-linked amniotic membranes for cultivation of limbal epithelial cells, Biomaterials 31 (2010) 6647–6658.
[46] L. Matilainen, T. Toropainen, H. Vihola, J. Hirvonen, T. Jarvinen, P. Jarho, K. Jarvinen, In vitro toxicity and permeation of cyclodextrins in Calu-3 cells, J. Control. Release 126 (2008) 10–16.
[47] A. Cestelli, C. Catania, S. D'Agostino, I. Di Liegro, L. Licata, G. Schiera, G.L. Pitarresi, G. Savettieri, V. De Caro, G. Giandalia, L.I. Giannola, Functional feature of a novel model of blood brain barrier: studies on permeation of test compounds, J. Control. Release 76 (2001) 139–147.
[48] D.P. Bakker, A. van der Plaats, G.J. Verkerke, H.J. Busscher, H.C. van der Mei, Comparison of velocity profiles for different flow chamber designs used in studies of microbial adhesion to surfaces, Appl. Environ. Microbiol. 69 (2003) 6280–6287.
[49] R. Cheng, Y.G. Lai, K.B. Chandran, Three-dimensional fluid-structure interaction simulation of Bileaflet mechanical heart valve flow dynamics, Ann. Biomed. Eng. 32 (2004) 1471–1483.